

Three-dimensional Cardiovascular Imaging-Genetics: A Mass Univariate Framework

Carlo Biffi,^{1,2} Antonio de Marvao,² Mark I. Attard,² Timothy J.W. Dawes,² Nicola Whiffin,^{2,3,4} Wenjia Bai,¹ Wenzhe Shi,¹ Catherine Francis,^{3,4} Hannah Meyer,⁵ Rachel Buchan,^{3,4} Stuart A. Cook,^{2,3,4,6,7} Daniel Rueckert,¹ and Declan P. O'Regan²

¹*Department of Computing, Imperial College London, South Kensington Campus, London, UK.*

²*MRC London Institute of Medical Sciences, Faculty of Medicine, Imperial College London, Hammersmith Hospital Campus, London, UK.*

³*National Heart and Lung Institute, Imperial College London, London, UK.*

⁴*NIHR Royal Brompton Cardiovascular Biomedical Research Unit, London, UK.*

⁵*European Molecular Biology Laboratory, European Bioinformatics Institute, Hinxton, UK.*

⁶*National Heart Centre Singapore, Singapore.*

⁷*Duke National University Singapore, Singapore.*

Background: Left ventricular (LV) hypertrophy is a strong predictor of cardiovascular outcomes, but its genetic regulation remains largely unexplained. Conventional phenotyping relies on manual calculation of LV mass and wall thickness, but advanced cardiac image analysis presents an opportunity for high-throughput mapping of genotype-phenotype associations in three dimensions (3D). **Methods:** High-resolution cardiac magnetic resonance images were automatically segmented in 1,124 healthy volunteers to create a 3D shape model of the heart. Mass univariate regression was used to plot a 3D effect-size map for the association between wall thickness and a set of predictors at each vertex in the mesh. The vertices where a significant effect exists were determined by applying threshold-free cluster enhancement to boost areas of signal with spatial contiguity. **Results:** Experiments on simulated phenotypic signals and SNP replication show that this approach offers a substantial gain in statistical power for cardiac genotype-phenotype associations while providing good control of the false discovery rate. **Conclusion:** This framework models the effects of genetic variation throughout the heart and can be automatically applied to large population cohorts.

Keywords: imaging-genetics, statistical parametric mapping, computational cardiac atlas.

I. INTRODUCTION

The concept that imaging phenotypes bear a close relationship to the underlying biology of disease has drawn considerable interest in neuroscience and is also now gaining traction for understanding the genetic and environmental predictors of cardiovascular disease¹. Novel three-dimensional (3D) cardiac imaging coupled with computational anatomic and functional modelling promise a means to better understand how environmental factors and genetic variants regulate specific morphological and functional traits in the heart².

One method of exploiting the rich biological information available in magnetic resonance (MR) images is to use atlas-based segmentation and co-registration where prior knowledge is used to annotate the images and represent derived phenotypic data in a standardized coordinate space (FIG. 1)³. This computational approach enables statistical modelling of the variation in 3D cardiac geometry but presents its own set of challenges for drawing inferences. One way to address the problem is to transform the spatially-correlated data into a smaller number of uncorrelated principal components, however these modes do not provide an explicit model relating genotype to phenotype³. A contrasting approach consists of deriving a statistic expressing evidence of a given effect at each and every point of the 3D model, hence cre-

ating a so-called statistical parametric map. Such mass univariate analyses have been extensively employed in functional neuroimaging studies to discover volumetric variations at vertex-wise level⁴. Its major advantage in neuroscience is to enable inferences about the function of localised brain regions in a computationally tractable way. On the other hand, this approach fails to regard dependence patterns between neighbouring points and causes a non-trivial multiple testing problem, resulting in a loss of statistical power. Many approaches have been attempted to address these limitations and particularly relevant for this work is threshold-free cluster enhancement (TFCE)⁵. TFCE is an image-enhancement technique that computes at each voxel a score based on the extent and magnitude of the area of coherent signal that surrounds it, making it possible to detect spatial effects with higher sensitivity by relying on the assumption that biological signal would create greater coherent areas of signal than noise.

Mass univariate analysis has only recently been applied to 3D cardiac imaging, and although the approach is feasible in population-based studies, it may provide overly-conservative inferences without considering spatial dependencies in the underlying data⁶⁻⁸. The aim of this paper is to introduce a general methodological approach for performing regression analyses on high-resolution cardiac MRI data - translating parametric statistical map-

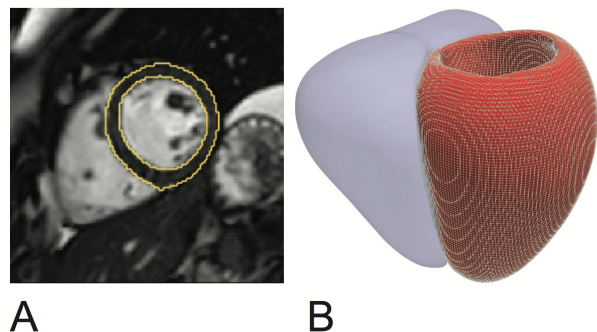


FIG. 1. **Computational image analysis.** (A) Short axis cardiac magnetic resonance image demonstrating automated segmentation of the endocardial and epicardial boundaries of the left ventricle (shown in yellow). (B) The segmentation is used to construct a three dimensional mesh of the cardiac surfaces (left ventricle shown in red, right ventricle in blue) that is co-registered to a standard coordinate space. Phenotypic parameters, such as wall thickness, are then derived for each vertex in the model.

ping approaches validated in neuroimaging to cardiovascular medicine. The proposed approach applies TFCE to population data enabling the detection of regional phenotype-genotype effects with strict multiple testing control. The feasibility of the proposed methodology to derive computationally-efficient inferences on imaging-genetics datasets has been tested through experiments on clinical and synthetic data using an R package developed for this purpose.

II. METHODS

A. Study population

The healthy volunteers dataset used in this study is part of the UK Digital Heart Project at Imperial College London⁹ (see Appendix A for full cohort characteristic and acquisition details). Participants who had known cardiovascular or metabolic disease were excluded. To capture the whole-heart phenotype, a high-spatial resolution 3D balanced steady-state free precession cine sequence Cardiac MR (CMR) was performed on a 1.5-T Philips Achieva system (Best, the Netherlands). Images were stored on an open-source database (MRIdb, Imperial College London, UK)¹⁰. Conventional volumetric analysis of the cine images was performed using CMR-tools (Cardiovascular Imaging Solutions, London, UK) following a standard protocol¹¹.

Genotyping of common variants was carried out using Illumina HumanOmniExpress-12v1-1 single nucleotide polymorphism (SNP) array (Sanger Institute, Cambridge). Clustering, calling and scoring of SNPs was performed using Illumina GenCall software. Samples were pre-phased with SHAPEIT¹² and imputation was performed using IMPUTE2¹³ with the UK10K dataset as a reference (www.uk10k.org). Quality of the genotypes was evaluated both on a per-individual and per-marker level using in-house Perl scripts. SNPs were removed

if they had a Impute information (INFO) score < 0.4 , missing call rate in more than 1% of samples, minor allele frequency of less than 1% or deviated significantly from Hardy-Weinberg equilibrium ($p > 0.001$). Only non-related individuals with "CEU" ethnicity were retained. The total genotyping rate in these individuals was 0.997 and the total number of variants available was 9.4 million.

B. Atlas-based segmentation and co-registration

All image processing was performed with Matlab (MathWorks, Natick, Mass). Briefly, a validated segmentation framework was used exploiting prior knowledge of cardiac anatomy from manually labelled atlases⁶. A multi-atlas approach was used in which the entire data set of labelled atlases was used for initial registration and then the 20 most similar atlases for final segmentation¹⁴. Initial alignment was estimated by registering six landmarks that were automatically detected using a decision forests method¹⁵. The alignment was then refined using non-rigid registration between target and atlas images¹⁶. Based on the spatial alignment, the atlas label maps were propagated onto the target image and combined to form the final segmentation using patch-based label fusion. A 3D mesh representing the mean endocardial and epicardial LV shapes at end-systole and end-diastole of the population dataset were obtained, and phenotypic variables calculated at 49,876 points on this surface (FIG. 1)⁹. Wall thickness (WT) was measured by computing the distance between respective vertices on the endocardial and epicardial surfaces at end-diastole.

C. Overview of the approach

In the following sections we introduce a framework for deriving associations between clinical/genetic parameters and a 3D cardiac phenotype. This approach can be summarized as shown in FIG. 2. Briefly, a general linear model is fitted at each vertex to extract the regression coefficient associated with the variable of interest (mass univariate regression). Threshold-free cluster enhancement (TFCE) is then applied to boost belief in extended areas of coherent signal in the derived vertex-wise statistical map. The points where a significant effect exists are determined by applying TFCE on the obtained t-statistic map and on N t-statistic maps obtained through permutation testing, derived under the null hypothesis of no effect. Then, at each vertex the frequentist probability of having obtained a higher TFCE score by chance is regarded as the p-value related to the regression coefficient β . Finally, the derived p-values are adjusted for multiple testing. The permutation testing procedure employed by this approach is the Freedman-Lane procedure¹⁷, whilst a false discovery rate (FDR) correction using the Benjamini-Hochberg procedure¹⁸ is applied to correct for multiple testing.

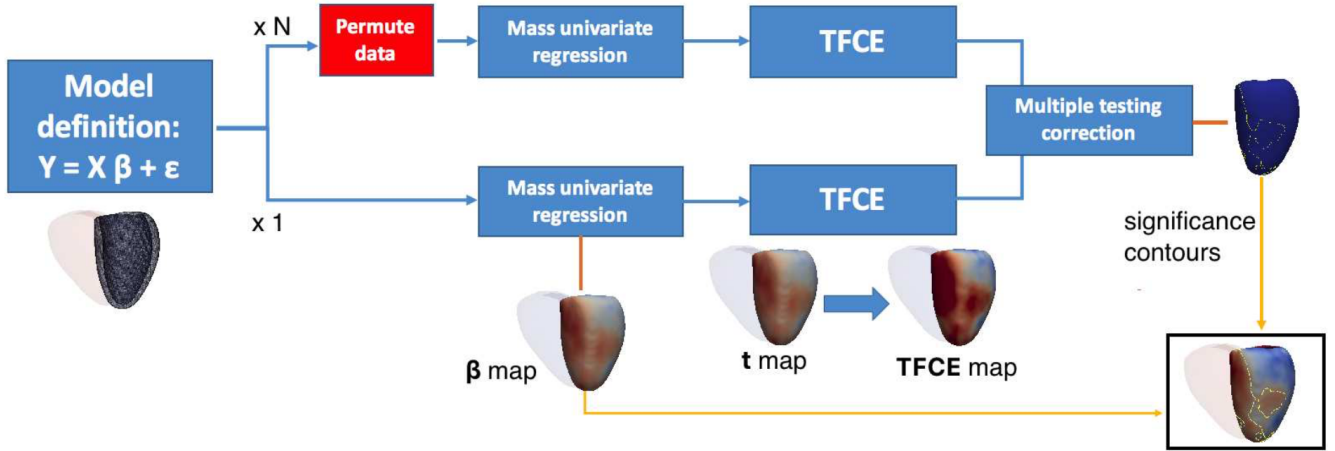


FIG. 2. **Outline of three-dimensional mass univariate framework.** A statistical atlas provides point-wise measures of ventricular geometry and function which can be linked to a given predictor through a general linear model. Using mass univariate regression, three-dimensional maps of a test statistic and the degree of association (β) can be derived. Threshold free cluster enhancement (TFCE) coupled with permutation testing produces vertex-wise p-values weighted to the degree of coherent spatial support. Finally, p-values are corrected for multiple testing. Regression coefficients enclosed by significance contours are represented on a model of the left ventricle.

D. Mass univariate analysis

The association between a ventricular phenotype mapped onto a cardiac atlas and one or more clinical variables can be described using a general linear model of the form $Y = \beta X + \epsilon$ where Y is a vector that stores the values of one ventricular phenotype (such as WT) at one anatomical point for all the subjects under study and X is a design matrix that can be used to model the effect under study and contains in each column the subject's values of a clinical variable as well as the intercept term. These variables can be numerical (such as age or weight), categorical or expressing interaction between them. In particular, categorical variables can be exploited to express either different categories (such as gender or ethnicity) or the presence/absence in a binary form of a clinical condition (such as the presence of genetic mutation or a specific disease). β is the regression coefficient vector to be estimated and ϵ represents the noise or error term, which is assumed to be a zero-mean Gaussian process and represents the variability of Y not explained by the model. The regression coefficient can be standardized by normalizing to mean 0 and unit-variance the columns of X and Y . As a result, β will represent the amount of variation of Y in units of its standard deviation when X is increased by one standard deviation, allowing comparisons between variables.

At each ventricular point of the cardiac atlas the same model can be fitted independently (mass univariate regression) and statistics can be extracted and corrected for multiple testing in order to test one or more statistical hypotheses. In a parametric framework, the t-statistic computed as $t = \frac{\beta}{s.e.(\beta)}$ is typically used in the neuroimaging literature to contrast the null hypothesis $H_0 : \beta = 0$ (no association between the predictor and the phenotype under study), where $s.e.(\beta)$ is the standard error of the estimator of β^4 . The regression coefficients β

and their related p-value thus obtained can be plotted on the atlas to display, at high resolution on the whole ventricle, the magnitude and spatial distribution of a given association. However, this approach underestimates associations where the signal is more spatially correlated than noise coherence. For this reason non-parametric statistics such as TFCE are valuable to increase the statistical power of the approach.

E. Threshold-free cluster enhancement on a cardiac atlas

The value of a statistic h obtained through mass univariate regression at a vertex p - a t-statistic in our context - is transformed by TFCE using the following integral:

$$TFCE(p) = \int_{h=0}^{h_p} e(h)^E h^H \delta h \simeq \sum_{h=0}^{h_p} e(h)^E h^H \Delta h \quad (1)$$

In the equation h_p is the value of the vertex statistic, $e(h)$ is the extent of the cluster with cluster-forming threshold h that contains p , and E and H are two parameters usually set to 0.5 and 2 for empirical and analytical motivations⁵. In computational algorithms the integral is estimated using a discrete sum. The computational model of the heart is defined as a 3D mesh composed of non-congruent triangles where at each vertex pointwise phenotypic variables are stored for each subject. The translation of TFCE to a cardiac model is not straightforward as the atlas is not composed of a regular grid of voxels (as in brain imaging applications) but instead forms a mesh of vertices. We addressed this problem by associating an area to each vertex i equivalent to the mesh area closer to the vertex i than to any other vertex in the mesh. In computing Eq. 1 at each vertex, the

most time consuming part is deriving $e(h)$ - the area of all the pixels connected to p that have a statistic value greater or equal to h - as a different $e(h)$ needs to be computed for each vertex of the mesh and for each term of the sum. However, the TFCE score associated to a vertex p of a specific h in the summation consists of the same score that should be associated with all the vertices which contribute to $e(h)$. Therefore, the computational time of the TFCE method can be significantly reduced by sampling the interval between the maximum and minimum statistic h in the statistic map so as to use each sampled value as a threshold \tilde{h} for the selection of vertices with a greater statistic value in the case of positive threshold, or less than \tilde{h} in the case of a negative thresholds. The edges of the graph are defined from a list containing the nearest neighbours of each vertex, and which is filtered at each iteration to contain only the vertices selected by the thresholding operation, resulting in one or more graphs of connected vertices. In this way, all the possible patterns of signal on the ventricle can be discovered without relying on assumptions about the geometry of cluster shapes. For all the obtained graphs including more than two vertices the TFCE score can be computed and associated to all the vertices that belong to them. The final TFCE score is the sum of all the TFCE scores thus obtained.

F. Permutation testing

The p-value associated with the regression coefficient computed at each atlas vertex can be derived via permutation testing. In particular, by permuting N times the input data, N TFCE scores maps can be obtained. It is important that the adopted permutation strategy guarantees the exchangeability assumption, *i.e.* permutations of Y given X do not alter the joint distribution of the dependent variables under the null hypothesis. In the proposed context, the Y values themselves are not exchangeable under the null hypothesis, as the predictors included in the model together with the variable under study are nuisance variables that could explain some portion of variability of Y . In order to address this problem, among all the different available techniques, the Freedman-Lane procedure¹⁷ has proved to provide the best control of statistical power and false positives (type 1 error)¹⁹. This procedure proceeds as follows. If Z contains all the nuisance variables previously contained in X , the general linear model can be rewritten as $Y = \beta X + \gamma Z + \epsilon$. Then, instead of permuting Y and extracting β , the procedure computes the residual-forming matrix $R_Z = 1 - XX^T$ and performs N different permutations by computing the model $\hat{P}_N R_Z Y = \beta X + \gamma Z + \epsilon$ at each point, where \hat{P}_N is the permutation operator. For a full derivation of the Freedman-Lane strategy see *Winkler et al.*¹⁹.

G. False discovery rate correction for multiple comparisons

A multiple testing problem arises by testing tens of thousands of statistical hypotheses simultaneously. Con-

trol of the family wise error rate at 5% could be derived by extracting the maximum score from each map derived via permutation testing and by using the 95th percentile as a threshold for significance. However, in this context such a correction could be overly conservative as we are rarely interested in the exact number of vertices that reaches significance. The main goal is to detect extended areas of coherent signal and therefore we can accept a maximum fixed percentage of false discoveries as provided by false discovery rate (FDR) procedures. In particular, these procedures can be applied to adjust the voxelwise p-values obtained at each vertex by computing the ratio between the number of times in which a TFCE score greater than the measured one has been obtained and the number of permutations N . We have found adaptive procedures such as the two-stage Benjamini-Hochberg²⁰ not suitable for our dataset, since it led to lower p-values and increased areas of significance, as also reported in the neuroimaging literature²¹. For this reason, the original Benjamini-Hochberg (BH)¹⁸ procedure has been employed for this work. It is important to underline that both FDR correction procedures are valid when the tested hypotheses are independent or satisfy a technical definition of dependence called positive regression dependency on a subset²². This condition for Gaussian data is translated into the requirement that the correlation between null voxels or between null and signal voxels is zero or positive, and for smoothed image data as those that compose a cardiac atlas, this assumption is generally considered satisfied⁴.

H. Software

We developed an R package available at <https://github.com/UK-Digital-Heart-Project/mutools3D> that provides functions to run a complete study. In the proposed code all the calculations are optimized using matrix algebra instead of exploiting built-in R functions, so as to avoid unnecessary operations and to benefit from the speed of vectorized operations. Linear regression assumptions must be met in order to obtain reliable inferences (for a review of them and their importance in a mass univariate setting see Appendix B), particularly important in this context are multicollinearity and heteroscedasticity problems which should be checked and solved for each model definition. For this latter, the R package implements mass univariate functions exploiting HC4m heteroscedascity consistent estimators²³.

III. RESULTS

A. TFCE improves the statistical power of the approach

As an exemplar application, 35 out of 52 SNPs which have been found associated with LVM in a genome wide association study (GWAS) meta-analysis of 73,518 individuals of European ancestry²⁴ were also identified in the UK Digital Heart Project genotypes and were assessed for replication. For each SNP, the association between

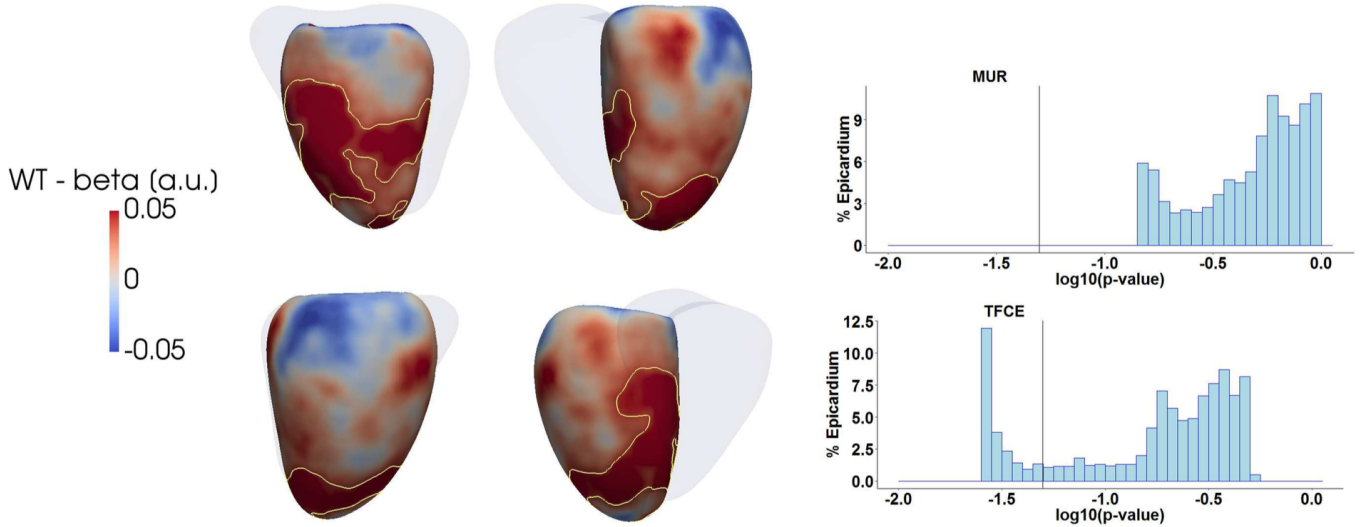


FIG. 3. **Applying three-dimensional analysis to single nucleotide polymorphism (SNP) replication.** On the left β coefficients are plotted on the surface of the left ventricle for the effect of rs7183401 on wall thickness (WT) adjusted for age, gender, body surface area and systolic blood pressure. Yellow contours enclose standardized regression coefficients reaching significance after multiple testing (FDR-BH) correction using the full pipeline. Standard mass univariate regression (MUR) did not provide any significant areas. The right ventricle is shown in outline for reference. On the right, the distributions of the derived p-values adjusted for multiple testing obtained with standard MUR or the proposed pipeline are shown (the vertical line represents $p\text{-value}=0.05$).

wall thickness (WT) at each vertex in the 3D model in 1,124 healthy Caucasian subjects was tested for association with the posterior estimate of the allele frequency by a regression model adjusted for age, gender, body surface area (BSA) and systolic blood pressure (SBP). The full list of the studied SNPs together with cohort characteristics is reported in Appendix C. Regression diagnosis through Breusch-Pagan and White’s test showed how the homoscedasticity assumption was violated at a large number of vertices, therefore mass univariate regression was corrected using HC4m heteroscedascity consistent estimators²³. Regarding the assumption of multicollinearity, the condition number of the model matrix was 2.19 while the variance inflation factor was equal to 1.06, suggesting a very low degree of multicollinearity. All the simulations were executed on a high performance computer (Intel Xeon Quad-Core Processor (30M Cache, 2.40 GHz), 36Gb RAM) and using the proposed R package. The number of permutations was set to 10,000 and each simulation required less than 6 hours.

Two SNPs, rs6565060 and rs7183401 showed a significant association with WT and the results for the latter are reported in FIG. 3. In particular, no vertices were significant without the application of TFCE, while the yellow-contoured areas enclose the significant vertices obtained by using the analysis pipeline proposed in this paper and shown in FIG. 2. The histogram on the right of FIG. 3 shows the distribution of derived FDR corrected p-values by applying the conventional mass univariate approach or by applying the full framework introduced by this work. TFCE enhanced areas of coherent signal which were predominantly in the inter-ventricular septum and apex. Conventional linear regression analysis using left ventricular mass (LVM) and the same model

did not reach significance ($\beta = -0.03$, $p = 0.43$).

B. Assessment of Sensitivity, Specificity and False Discovery Rate on Synthetic Data

Sensitivity, specificity and the rate of false discoveries of the proposed pipeline with or without the application of TFCE were estimated using synthetic data. From the previous clinical application, the 3D model showing no correlation between WT and the posterior estimate of the allele frequency of the rs4288653 SNP (X_{snp}) adjusted for age, gender, BSA and SBP was used to generate background noise. A synthetic data signal was generated by summing to the WT values of each subject a term $I \beta X_{snp}$ at each vertex, where I is the signal intensity and β is a map of regression coefficients. Two different β maps obtained from real clinical data were employed as shown on the left side of FIG. 4. The first (signal a) was obtained by fitting a 3D regression model associating WT adjusted for ventricular volume and systolic blood pressure in 134 hypertensive subjects of the UK Digital Heart dataset. The 2,498 significant regression coefficients obtained out of a total of 29,298 were then scaled to the $(0,1]$ range, while the others were set to 0. The second map (signal b) was obtained by extracting the 17,746 significant positive regression coefficients obtained in the exemplar application of the previous section (FIG. 3), and by scaling them to the $[-1,0)$ range to generate this time a more extended and negative sign signal. By subsampling the number of subjects to study N and the signal intensity I , different signals to be detected by our proposed standard mass univariate pipeline with or without TFCE enhancement were obtained. The number

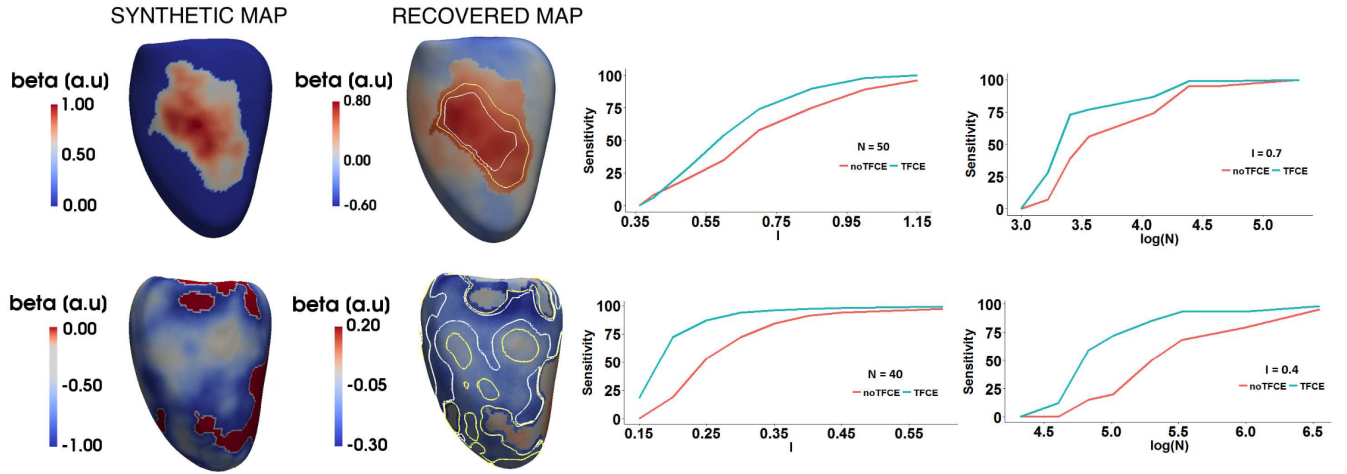


FIG. 4. **Model assessment using synthetic data.** First row (signal a) - beta coefficients used to generate the synthetic signal (2,498 vertices with positive coefficients), example of result ($I=0.85$ and $N=50$, significant vertices derived using TFCE contoured in yellow, without TFCE in white), sensitivity results at different signal intensities I and sample sizes N . Second row (signal b) - beta coefficients used to generate the synthetic signal (17,746 vertices with negative coefficients), example of result ($I=0.25$ and $N=40$, significant vertices derived using TFCE contoured in yellow, without TFCE in white), sensitivity results at different signal intensities I and sample sizes N .

of permutations for each simulation was fixed to 5,000. As reported in FIG. 4, sensitivity increased at larger sample sizes N and signal intensities I . Overall, the application of TFCE produced a substantial increase in the sensitivity of the approach, especially on the most extended signal (signal b) reported in the second row of FIG. 4. Moreover, a strict control on the rate of false discoveries was kept as can be seen in the specificity and FDR plots reported in Appendix D - where the FDR was always below 5% and often below 1%.

IV. DISCUSSION

The environmental and genetic determinants of cardiac physiology and function, especially in the earliest stages of disease, remain poorly characterized and morphological classification relies on one-dimensional metrics derived by manual image segmentation²⁵. In this paper, we have introduced a general linear model framework that provides a powerful approach for modelling the relationship between phenotypic traits and environmental and genetic factors using high-fidelity 3D representations of the heart. By translating statistical parametric mapping techniques originally developed for brain mapping to the cardiovascular domain we exploit spatial dependencies in the data to identify coherent areas of biological effect in the myocardium. This framework also accounts for multiple testing correction at tens of thousands of vertices which is the main drawback of this class of techniques. In particular, the application of TFCE leads to a notable increase in power of the mass univariate approach at the expense of only a slight increase of the false discovery rate - which is not biologically significant in extent. In the exemplar application reported, we replicated the effect of a SNP discovered in a GWAS for LVM²⁴, where significance was only reached using a 3D WT phenotype

with TFCE applied. The rs7183401 allele, corresponding to the alpha kinase 3 (ALPK3) gene, was recently implicated in early-onset cardiomyopathy in humans²⁶. The same model did not reach significance when tested against LVM in a conventional linear regression setting, underlining the importance of mass univariate approaches in studying regional effects, instead of reducing the information provided by cardiovascular imaging to a few manually-derived volumetric parameters.

Genetic association studies using conventional 2D imaging leave much of the moderate heritability of LVM unexplained²⁷⁻²⁹. One contribution may be the lack of phenotyping power of conventional imaging metrics of volumes and mass, which require manual analysis and are insensitive to regional patterns of hypertrophy. The proposed methodology represents a more powerful approach which maps at high-resolution the anatomic variation in cardiovascular geometry associated with environmental factors and genetic variants in a linear regression model. As well as common variants, this approach also shows potential for revealing the effect of rare variants on LV geometry in participants without overt cardiomyopathy³⁰. Despite the increased statistical power provided by TFCE, the multiple testing problem that arises by computing a large number of univariate models and the failure to regard the covariance across neighbouring vertices could be still considered an important drawback of the approach. As an alternative, multivariate approaches have increased efficiency and statistical power but this comes at the price of increased computational burden and more complex topological interpretation³¹. The same consideration is valid regarding the use of the general linear model: despite the fact that the true association may not be linear in the model parameters, the advantages provided by its simplicity, ability to easily design and adjust the results for multiple factors, the strong statistical background related to it and the fact that it is still

one of the most widely used models for statistical analysis in biomedical research, favour its use. A limitation is that high-spatial resolution CMR is not available in all cohorts, although conventional two-dimensional images may be interpolated to provide similar shape models³². As the methods are computationally-efficient and require no human input for phenotypic analysis, it is feasible to scale up the pipeline to larger population cohorts such as UK Biobank, which aims to investigate up to 100,000 participants using MR imaging³³. Applying these concepts to cardiovascular GWAS replication and candidate gene studies is appealing as 3D phenotypic traits may have a stronger relationship to genetic variation than conventional global volumetric parameters³⁴. While we have focused on LV geometry and shape, the same approach can be applied to time-resolved vertex-wise data to create a functional phenotype for regression modelling.

V. CONCLUSION

We report a powerful and flexible framework for statistical parametric modelling of 3D cardiac atlases, encoding multiple phenotypic traits, which offers a substantial gain in power with robust inferences. We have implemented and validated the approach on both synthetic and clinical datasets, showing its suitability for detecting genotype-phenotype interactions on LV geometry. More generally, the proposed method can be applied to population-based studies to increase our understanding of the physiological, genetic and environmental effects on cardiac structure and function.

ACKNOWLEDGMENTS

The authors thank Dr. James Ware for advice on GWAS replication; our radiographers Ben Statton, Marina Quinlan and Alaine Berry; our research nurses Tamara Diamond and Laura Monje Garcia; and the study participants.

FUNDING

The study was supported by the Medical Research Council, UK; National Institute for Health Research (NIHR) Biomedical Research Centre based at Imperial College Healthcare NHS Trust and Imperial College London, UK; British Heart Foundation grants PG/12/27/29489, NH/17/1/32725, SP/10/10/28431 and RE/13/4/30184; Academy of Medical Sciences Grant (SGL015/100) and a Wellcome Trust-GSK Fellowship Grant (100211/Z/12/Z).

APPENDICES

Appendix A: UK Digital Heart Project protocols

Participants who had known cardiovascular or metabolic disease or were taking prescription medicines were excluded but simple analgesics, antihistamines, and oral contraceptives were acceptable. Female subjects were excluded if they were pregnant or breastfeeding. Standard safety contraindications to magnetic resonance imaging were applied including a weight limit of 120 kg. All subjects provided written informed consent for participation in the study, which was approved by a research ethics committee. Anthropometric measurements were collected by trained research nurses. Subjects fasted for four hours before the visit took place. Blood pressure was acquired in accordance with the guidelines of the European Society of Hypertension³⁵ using a calibrated oscillometric device (Omron M7, Omron Corporation, Kyoto, Japan). Five measures were taken, the first three were discarded and the last two were averaged. Subjects height (Ht) and weight (Wt) were assessed without shoes and body surface area (BSA) was calculated by the

Mosteller formula: $BSA(m^2) = \sqrt{\frac{Ht(cm) * Wt(kg)}{3600}}$.

Cardiac MR (CMR) was performed on a 1.5-T Philips Achieva system (Best, the Netherlands). To capture the whole-heart phenotype, a high-spatial resolution 3D balanced steady-state free precession cine sequence was used that assessed the left and right ventricles in their entirety in a single breath-hold (60 sections, repetition time 3.0 ms, echo time 1.5 ms, flip angle 50°, field of view 320 × 320 × 112 mm, matrix 160 × 95, reconstructed voxel size 1.2 × 1.2 × 2 mm, 20 cardiac phases, temporal resolution 100 ms, typical breath-hold 20 s). Images were stored on an open-source database (MRIdb, Imperial College London, UK)¹⁰. Conventional volumetric analysis of the cine images was performed using CMRtools (Cardiovascular Imaging Solutions, London, UK) following a standard protocol¹¹.

Appendix B: Gauss-Markov assumptions

In this section we review the statistical assumptions of the general linear model and their importance in a mass univariate context, so as to clarify under which conditions reliable inference can be obtained.

The regression coefficients β in the general linear model under study can be obtained via ordinary least squares (OLS): $\beta = (XX^T)^{-1}X^T y$ and $s.e.(\beta) = \sqrt{s^2(XX^T)^{-1}}$, where s^2 is the OLS estimate of the variance σ^2 of the observations. According to the Gauss-Markov theorem, the ordinary least square method will be the best linear unbiased estimator (BLUE) of the regression coefficients β if its five assumptions are satisfied. Here we report the importance of these assumptions for the approach proposed in this work.

1. *No multicollinearity in X.* Multicollinearity is present when a covariate is a linear combination (perfect) or is highly correlated (imperfect) with

other covariates. The absence of perfect collinearity is necessary to guarantee that X is full rank so that XX^T can be inverted when deriving the regression coefficients, assuring their uniqueness. Imperfect multicollinearity results in a reduction of the statistical efficiency of the derived regression coefficients, causing a reduction of power and ambiguous effects³⁶. In order to diagnose this, low pairwise correlations between predictor variables are not sufficient to exclude multicollinearity with more than two explanatory variables, but they are a necessary condition. The variance inflation factor and the condition number of the design matrix can be instead employed to estimate the amount of variance of each regression coefficient increased because of collinearity and to detect the amount of collinearity respectively³⁷. Taking together these three latter indices, modifications of the design matrix via omission or orthogonalization of explanatory variables can be considered to correct for multicollinearity.

2. *Random sampling of the population.* This assumption is required in order to not introduce bias in the estimates and it is guaranteed when candidates have been randomly selected to participate to the study.
3. *No endogeneity in X.* Endogeneity happens when an explanatory variable is correlated with the error term, *i.e.* $E(\epsilon_i|X) \neq 0$. In general, this problem can be due to a model misspecification problem where one or more predictors have not been included into the model, to a measurement error in X that will add bias to the estimation of the regression coefficients, or to a simultaneity error when one column of X is jointly determined with Y. As endogeneity is a conceptual problem, there are no direct statistical tests to verify this assumption, hence the results should be questioned each time. In the context under study, the last source of endogeneity can be considered negligible as imaging and clinical data comes from different sources. Bias due to measurement errors should be considered and addressed in the experimental design definition. Finally, the first assumption implies that the proposed approach can only prove association and not cause-effect relationships.
4. *Linearity and additivity.* The relation between dependent and independent variables is required to be linear in the parameters β , therefore this assumption requires the model covariates to be correctly specified. More importantly it is required that the independent variables are additive, *i.e.* the amount of change in Y associated with the increase of one predictor is independent of the values of the other covariates. This latter assumption guarantees the correct interpretation of the obtained regression coefficients, avoiding their overestimation. In our context, non-additivity can be addressed by defining interaction terms of the predictors. Moreover, when interpreting the derived regression coef-

ficients, this assumption highlights again that this approach only shows the presence of associations and not cause-effect relationships.

5. *Homoscedasticity.* This assumption requires that the error variance σ is identical across observations. It can be tested by computing a heteroscedasticity test such as the Breusch-Pagan (for linear heteroscedasticity) or the White's test (for non-linear heteroscedasticity). Heteroscedasticity causes too wide or too narrow regression coefficient standard errors, giving too much weight to certain subsets of the data when estimating the β s. Important sources of this effect rely in physiological or artifactual effects that underlie the measurements and they can be reduced by using either using weighted least squares, log transformations of the data or heteroscedasticity-consistent robust standard errors.

If assumptions 1-4 are valid the estimation of the regression coefficients are unbiased and consistent, and if 5 is also valid it becomes efficient.

Appendix C: Exemplar application supplementary data

The list of 35 SNPs tested from *van der Harst et al.*²⁴ paper is the following: rs17391905, rs2207790, rs2274317, rs12036340, rs10920184, rs4288653, rs6710065, rs3770770, rs3816849, rs2242285, rs13314892, rs1344852, rs13185595, rs1015150, rs11153730, rs11773845, rs10105974, rs1733724, rs12414364, rs10509289, rs7099599, rs2269434, rs736825, rs2926743, rs1408224, rs7183401, rs6565060, rs7211246, rs242562, rs617759, rs879568, rs10853525, rs3929778, rs2025096 and rs13047360.

Table I contains a summary of the covariates employed in the adopted regression model.

Appendix D: Specificity and False Discovery Rate on Synthetic Data

In FIG. 5 and FIG. 6 we report specificity and FDR results of the proposed pipeline with or without the application of TFCE using synthetic data at different signal intensities I and sample sizes N. β coefficients used to generate the synthetic signal and examples of results are reported in FIG. ??.

	Full Cohort ($N = 1,124$)	Males ($N = 511$)	Females ($N = 613$)
Age [years]	43.4 ± 13.3 (19-77)	43.2 ± 13.0 (19-77)	43.5 ± 13.2 (20-77)
BSA [m^2]	1.84 ± 0.2	1.98 ± 0.16	1.72 ± 0.14
SBP [mmHg]	119.3 ± 14	125.0 ± 12.7	114.65 ± 13.2

TABLE I. A summary of the 1,124 Caucasian subjects of UK Digital Heart Project at Imperial College cohort whose MRI scans has been used in this work.

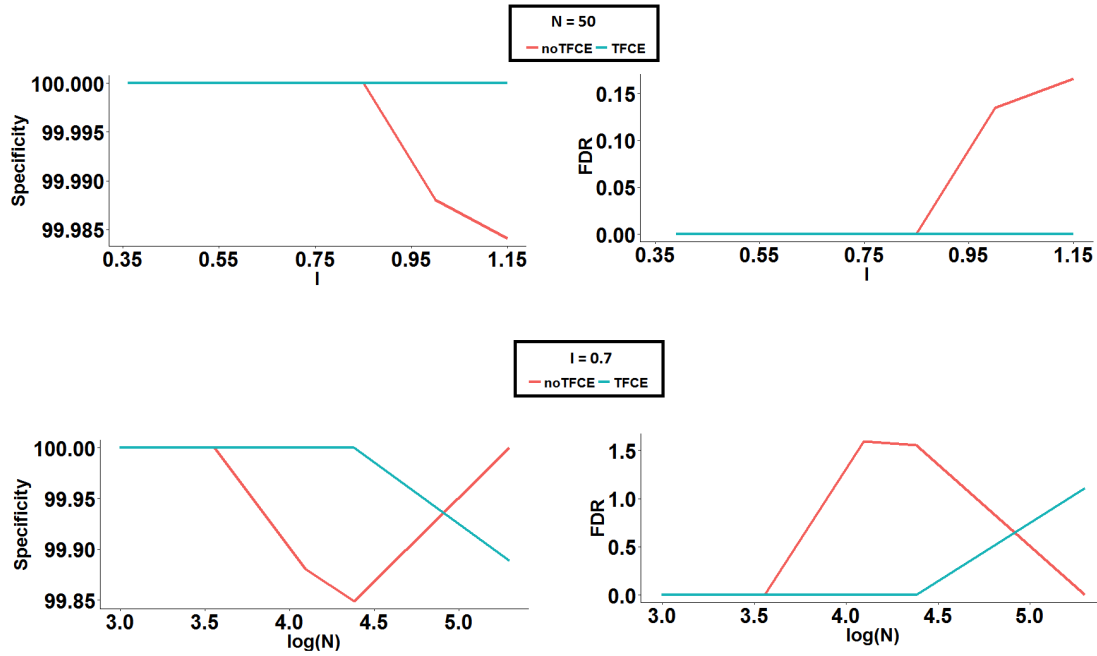


FIG. 5. Signal a. Assessment of specificity and FDR of the proposed pipeline with or without the application of TFCE using synthetic data generated at different signal intensities I and sample sizes N .

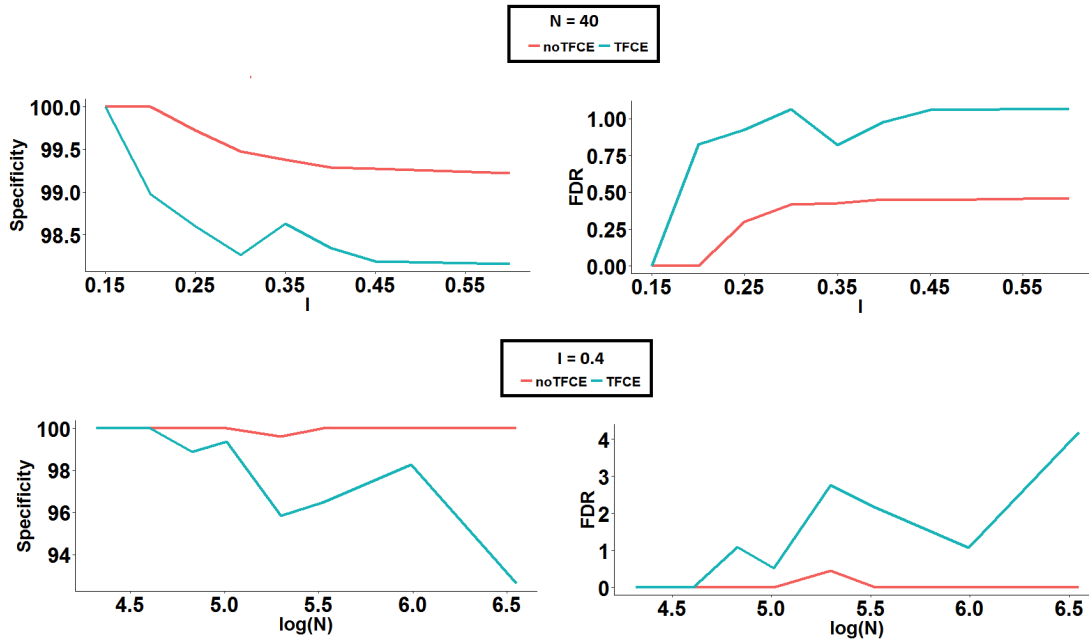


FIG. 6. Signal b. Assessment of specificity and FDR of the proposed pipeline with or without the application of TFCE using synthetic data generated at different signal intensities I and sample sizes N .

REFERENCES

- ¹J. Flint and M. R. Munafò, “The endophenotype concept in psychiatric genetics,” *Psychol Med* **37**, 163–180 (2007).
- ²A. de Marvao *et al.*, “Population-based studies of myocardial hypertrophy: high resolution cardiovascular magnetic resonance atlases improve statistical power,” *J Cardiovasc Magn Reson* **16**, 16 (2014).
- ³A. A. Young and A. F. Frangi, “Computational cardiac atlases: from patient to population and back,” *Exp Physiol* **94**, 578–596 (2009).
- ⁴W. D. Penny *et al.*, *Statistical parametric mapping: the analysis of functional brain images* (Academic press, 2011).
- ⁵S. M. Smith and T. E. Nichols, “Threshold-free cluster enhancement: addressing problems of smoothing, threshold dependence and localisation in cluster inference,” *NeuroImage* **44**, 83–98 (2009).
- ⁶A. de Marvao *et al.*, “Precursors of hypertensive heart phenotype develop in healthy adults: a high-resolution 3D MRI study,” *JACC Cardiovasc Imaging* **8**, 1260–1269 (2015).
- ⁷B. Corden *et al.*, “Relationship between body composition and left ventricular geometry using three dimensional cardiovascular magnetic resonance,” *J Cardiovasc Magn Reson* **18**, 32 (2016).
- ⁸M. De Craene *et al.*, “SPM to the heart: mapping of 4D continuous velocities for motion abnormality quantification,” in *2012 9th IEEE International Symposium on Biomedical Imaging (ISBI)* (IEEE, 2012) pp. 454–457.
- ⁹W. Bai *et al.*, “A bi-ventricular cardiac atlas built from 1000+ high resolution MR images of healthy subjects and an analysis of shape and motion,” *Med Image Anal* **26**, 133–145 (2015).
- ¹⁰M. Woodbridge *et al.*, “MRIdb: medical image management for biobank research,” *J Digit Imaging* **26**, 886–890 (2013).
- ¹¹J. Schulz-Menger *et al.*, “Standardized image interpretation and post processing in cardiovascular magnetic resonance: Society for Cardiovascular Magnetic Resonance (SCMR) board of trustees task force on standardized post processing,” *J Cardiovasc Magn Reson* **15**, 35 (2013).
- ¹²O. Delaneau, J.-F. Zagury, and J. Marchini, “Improved whole-chromosome phasing for disease and population genetic studies,” *Nat Methods* **10**, 5–6 (2013).
- ¹³B. N. Howie, P. Donnelly, and J. Marchini, “A flexible and accurate genotype imputation method for the next generation of genome-wide association studies,” *PLoS Genet* **5**, e1000529 (2009).
- ¹⁴P. Aljabar *et al.*, “Multi-atlas based segmentation of brain images: atlas selection and its effect on accuracy,” *NeuroImage* **46**, 726–738 (2009).
- ¹⁵O. Oktay *et al.*, “Stratified decision forests for accurate anatomical landmark localization in cardiac images,” *IEEE Trans Med Imaging* **36**, 332–342 (2017).
- ¹⁶D. Rueckert *et al.*, “Nonrigid registration using free-form deformations: application to breast MR images,” *IEEE Trans Med Imaging* **18**, 712–721 (1999).
- ¹⁷D. Freedman and D. Lane, “A nonstochastic interpretation of reported significance levels,” *Journal of Business & Economic Statistics* **1**, 292–298 (1983).
- ¹⁸Y. Benjamin and Y. Hochberg, “Controlling the false discovery rate: a practical and powerful approach to multiple testing,” *J Royal Statistical Society, Series B* (57) **289** (1995).
- ¹⁹A. M. Winkler *et al.*, “Permutation inference for the general linear model,” *NeuroImage* **92**, 381–397 (2014).
- ²⁰Y. Benjamini *et al.*, “Adaptive linear step-up procedures that control the false discovery rate,” *Biometrika* **93**, 491–507 (2006).
- ²¹P. T. Reiss *et al.*, “Paradoxical results of adaptive false discovery rate procedures in neuroimaging studies,” *NeuroImage* **63**, 1833–1840 (2012).
- ²²Y. Benjamini and D. Yekutieli, “The control of the false discovery rate in multiple testing under dependency,” *Ann Stat*, 1165–1188 (2001).
- ²³F. Cribari-Neto and W. B. da Silva, “A new heteroskedasticity-consistent covariance matrix estimator for the linear regression model,” *AStA Adv Stat Anal* **95**, 129–146 (2011).
- ²⁴P. van der Harst *et al.*, “52 genetic loci influencing myocardial mass,” *J Am Coll Cardiol* **68**, 1435–1448 (2016).
- ²⁵M. G. Khouri *et al.*, “A 4-tiered classification of left ventricular hypertrophy based on left ventricular geometry the Dallas heart study,” *Circ Cardiovasc Imaging* **3**, 164–171 (2010).
- ²⁶R. Almomani *et al.*, “Biallelic truncating mutations in ALPK3 cause severe pediatric cardiomyopathy,” *J Am Coll Cardiol* **67**, 515–25 (2016).
- ²⁷R. S. Vasani *et al.*, “Genetic variants associated with cardiac structure and function: a meta-analysis and replication of genome-wide association data,” *JAMA* **302**, 168–178 (2009).
- ²⁸E. R. Fox *et al.*, “Genome-wide association study of cardiac structure and systolic function in African Americans: the Candidate Gene Association Resource (CARE) study,” *Circ Cardiovasc Genet* **6**, 37–46 (2013).
- ²⁹C. Semsarian *et al.*, “New perspectives on the prevalence of hypertrophic cardiomyopathy,” *J Am Coll Cardiol* **65**, 1249–1254 (2015).
- ³⁰S. Schafer *et al.*, “Titin-truncating variants affect heart function in disease cohorts and the general population,” *Nature Genet* **49**, 46–53 (2017).
- ³¹C. Habeck *et al.*, “Multivariate data analysis for neuroimaging data: overview and application to Alzheimer’s disease,” *Cell Biochem Biophys* **58**, 53–67 (2010).
- ³²W. Shi *et al.*, “Cardiac image super-resolution with global correspondence using multi-atlas patchmatch,” *Med Image Comput Comput Assist Interv* **16**, 9–16 (2013).
- ³³S. E. Petersen *et al.*, “Imaging in population science: cardiovascular magnetic resonance in 100,000 participants of UK Biobank—rationale, challenges and approaches,” *J Cardiovasc Magn Reson* **15**, 1 (2013).
- ³⁴T. Ge *et al.*, “Increasing power for voxel-wise genome-wide association studies: the random field theory, least square kernel machines and fast permutation procedures,” *NeuroImage* **63**, 858–873 (2012).
- ³⁵O’Brien *et al.*, “Working Group on Blood Pressure Monitoring of the European Society of Hypertension International Protocol for validation of blood pressure measuring devices in adults,” *Blood Press Monit* **7**, 3–17 (2002).
- ³⁶A. Andrade *et al.*, “Ambiguous results in functional neuroimaging data analysis due to covariate correlation,” *NeuroImage* **10**, 483–486 (1999).
- ³⁷J. F. Hair, ed., *Multivariate data analysis*, 7th ed. (Prentice Hall, 2010).